AAPS PharmSciTech, Vol. 11, No. 3, September 2010 (© 2010)
DOI: 10.1208/s12249-010-9516-7

Research Article

Analysis of Process Parameters Affecting Spray-Dried Oily Core Nanocapsules Using Factorial Design

Tao Zhang[1] and Bi-Botti C. Youan[1,2]

Received 11 March 2010; accepted 16 August 2010; published online 15 September 2010

Abstract. The purpose of this work was to optimize the process parameters required for the production of spray-dried oily core nanocapsules (NCs) with targeted size and drug yield using a two-level four-factor fractional factorial experimental design (FFED). The coded process parameters chosen were inlet temperature (X_1), feed flow rate (X_2), atomizing air flow (X_3), and aspiration rate (X_4). The produced NCs were characterized for size, yield, morphology, and powder flowability by dynamic light scattering, electron microscope, Carr's index, and Hausner ratio measurement, respectively. The mean size of produced NCs ranged from 129.5 to 444.8 nm, with yield varying from 14.1% to 31.1%. The statistical analysis indicated an adequate model fit in predicting the effect of process parameters affecting yield. Predicted condition for maximum yield was: inlet temperature 140°C, atomizing air flow 600 L/h, feed flow rate 0.18 L/h, and aspiration air flow set at 100%, which led to a yield of 30.8%. The morphological analysis showed the existence of oily core and spherical nanostructure. The results from powder flowability analysis indicated average Carr's index and Hausner ratio of 42.77% and 1.76, respectively. Spray-dried oily core NCs with size lower than 200 nm were successfully produced, and the FFED proved to be an effective approach in predicting the production of spray-dried NCs of targeted yield.

KEY WORDS: fractional factorial design; indomethacin; oily core nanocapsules; process variables; spray drying.

INTRODUCTION

The concept of nanocapsules (NCs) was first introduced in 1977 (1). NCs present a core–shell structure with either an aqueous or oily core surrounded by a polymeric shell. In contrast to nanosphere (NP), which was identified as a continuous polymeric matrix, NCs have several advantages. For example, (1) the loading efficiency of poorly water soluble drugs can be significantly improved; (2) the drug can be encapsulated in a central cavity, avoiding the possible drug adsorption on the NP surface, which is common during NP preparation (2,3). Therefore, the burst effect due to surface adsorption could be minimized; (3) reduced irritation because drug is not in direct contact with the site of action; (4) protect the drug from degradation during both storage and after administration (4). Therefore, NCs are under extensive study and proved to be a promising vector for lipophilic drugs (5,6).

Spray drying is a widely applied technique for producing a dry powder form from a liquid by rapidly drying with hot gas. The concept of spray drying has been extensively applied in the drying of various pharmaceutical excipients (7–9). This technology exhibits several advantages: drying in a rapid one-step process, comparable low price with easy scale-up, suitable with heat sensitive molecules such as enzymes and proteins, and the possibility of modulating powder characteristics such as size by process analytical technology (10). A series of methods for spray-drying polymeric NCs and NP have been proposed and studied, with appropriate spray-drying adjuvant (11,12). For the operator of the spray-drying process, several major process parameters which may have direct influence on product quality should be considered and controlled, such as: the inlet temperature of the drying air, the drying air flow rate, the supply rate of the feed liquid, and the pressure/volume of the atomizing air as well as the drying air flow (13). Therefore, the process parameters in the spray-drying technique should be carefully controlled in order to avoid unwanted consequences such as particle aggregation, low yield, and high moisture content. Previous literatures have focused on the effect of process parameters during spray drying and/or spray congealing process (14–17). Although NCs around 200 nm have been successfully prepared by spray drying (12,18,19), there is a knowledge gap on the systematic and statistical analysis of the effect of process parameters, specifically during spray drying of oily core NCs. Thus, this study was designed to bridge this gap.

Design of experiments (DOE) is a component of quality-by-design (QbD), which is a systemic and simultaneous evaluation of variables in order to develop a desired product (20). Our group has recently combined the concept of DOE with nanoformulation (21,22). It is highly expected that by a useful statistical experimental design tool, one can understand the effects of process parameters and their interactions, which can be associated with quality attributes of the final product.

[1] Laboratory of Future Nanomedicines and Theoretical Chronopharmaceutics, Division of Pharmaceutical Sciences, University of Missouri-Kansas City, Kansas, Missouri 64108, USA.
[2] To whom correspondence should be addressed. (e-mail: youanb@umkc.edu)

Fractional factorial experiment designs (FFED) are experimental designs consisting of a fraction of the experimental runs of a full-factorial design. For example, in a two-level, four-factor FFED (2^{4-1} design), three factors (A, B, C) will go through every possible combination of high/low values as in a 2^3 design, while the fourth factor D will be constructed as D=ABC, respectively (23). This gives a total of eight runs compared to 16 runs in a full two-level–four-factor factorial design. FFED is good for screening experiments and to find out important variables from a large variable list (23).

Previously, our research group has successfully utilized Box–Behnken design to predict and optimize the formulation variables in spray-dried oily core NCs (data not shown). That previous study instead focused on the formulation variables (e.g., amount of polymer, oil, and surfactant) in order to minimize size and maximize encapsulation efficiency. However, the produced NCs exhibited relatively large size (>220 nm, not suitable for sterile filtration and i.v. administration) and low process yield. In this present study, the influence of four different process parameters was studied using 2^{4-1} FFED in order to overcome these limitations.

MATERIAL AND METHODS

Materials

Poly(D,L-lactide) Resomer® R208 was supplied by Boehringer Ingelheim Inc. (Ingelheim, Germany). Labrafac CC (caprylic/capric triglyceride) was kindly supplied by Gattefosse Corporation (Saint-Priest, France) as a gift. Poloxamer 407 (Pluronic F127) was a gift from Baden Aniline and Soda Factory Corporation (Ludwigshafen, Germany). Indomethacin (IND) was purchased from Sigma Aldrich (St. Louis, MO, USA). α-Lactose and ethyl acetate were purchased from Fisher Scientific (Fair Lawn, NJ, USA). All other chemicals used in this study were of analytical grade and used without further purification.

2^{4-1} Experimental Design

In this study, four process parameters, namely, inlet temperature, feed flow rate, atomizing air flow, and aspiration rate were selected at their low (coded −1) and high (coded +1) levels with triplicate centerpoints. The centerpoints provide a check for curvature and a measure of process stability and inherent variability (24). Therefore, it is recommended to add approximately three to five centerpoints to a full or fractional factorial design (25). The independent and dependent variables and their coded factors are listed in Table I. The equation obtained by statistical software (JMP 8, SAS Institute) was as follows:

$$Y_i = b_0 + b_1X_1 + b_2X_2 + b_3X_3 + b_4X_4 + b_{12}X_1X_2 + b_{13}X_1X_3 + b_{14}X_1X_4 \quad (1)$$

Where Y_i was the dependent variable; X_1 through X_4 were independent variables; b_0 was the intercept with y-axis; and b_1 through b_{14} were regression coefficients. In FFED, every two-factor interaction is aliased with another two-factor interaction, and those relationships are $X_1X_2=X_3X_4$, $X_1X_3=X_2X_4$, and $X_2X_3=X_1X_4$ (23). In this study, the independent variables were chosen based on preliminary experiments.

Table I. Variables and Their Levels in 2^{4-1} Design

Independent variables	Levels		
	Low	High	Centerpoints
X_{A1}=inlet temperature (°C)	140	150	145
X_{A2}=feed flow rate (L/h)	0.18	0.36	0.27
X_{A3}=atomizing air flow (L/h)	450	600	525
X_{A4}=aspiration rate (%) [a]	80	100	90
Coded values (X_1, X_2, X_3, X_4)	−1	+1	0
Dependent Variables			
Y_1=Particle size (nm)			
Y_2=Yield (%)			

[a] Aspiration rate represented the percentage of the maximum drying gas flow (35,000 L/h) of the Buchi B 290 spray dryer

Preparation of IND-Loaded Oily Core Nanocapsules Suspension

The IND-loaded oily core nanocapsules were prepared by an adopted emulsion–diffusion technique previously described by Quintanar-Guerreo *et al.* (26). First, mutually saturated deionized water and ethyl acetate were prepared by mixing deionized water and ethyl acetate and left settled overnight. Then, these two solvents were separated using a funnel. One hundred milligram of PLA was dissolved in 10 ml of water saturated ethyl acetate, and meanwhile, 360 mg of Pluronic F127 was dissolved in 40 ml of ethyl acetate saturated water. Then, 0.7 ml of Labrafac CC (oil) containing 10 mg of IND was added to the above water saturated ethyl acetate. The resulting organic phase was then poured into the water phase and emulsified with a homogenizer (IKA ULTRA-TURRAX T-25, Staufen, Germany) at 9,500 rpm for 10 min in which the oil-in-water emulsion was formed. Then, by adding deionized water (200 ml) to the emulsion under gentle stirring, ethyl acetate was extracted from the emulsion droplet, thus facilitating the precipitation and formation of NCs.

Spray-Drying of the IND-Loaded Oily Core Nanocapsules

The NCs powder was obtained by spraying the emulsion in previous step (adding 3% α-lactose as bulking agent) through

Table II. Response Values of Size (Y_1) and Yield (Y_2)

Run no.	X_1	X_2	X_3	X_4	Y_1 (nm)	PI	Y_2 (%)
1	+1	+1	−1	−1	150.3	0.199	19.7
2	+1	−1	−1	+1	264.0	0.291	18.3
3	−1	+1	−1	+1	201.9	0.251	19.7
4	+1	+1	+1	+1	153.4	0.162	28.5
5	−1	−1	+1	+1	129.5	0.121	31.1
6	0	0	0	0	149.6	0.148	22.7
7	0	0	0	0	151.7	0.211	23.5
8	0	0	0	0	153.8	0.200	21.4
9	+1	−1	+1	−1	167.4	0.231	31.1
10	−1	−1	−1	−1	208.6	0.157	14.1
11	−1	+1	+1	−1	444.8	0.304	25.5

X_1 inlet temperature, X_2 feed flow rate, X_3 atomizing air flow, X_4 aspiration rate

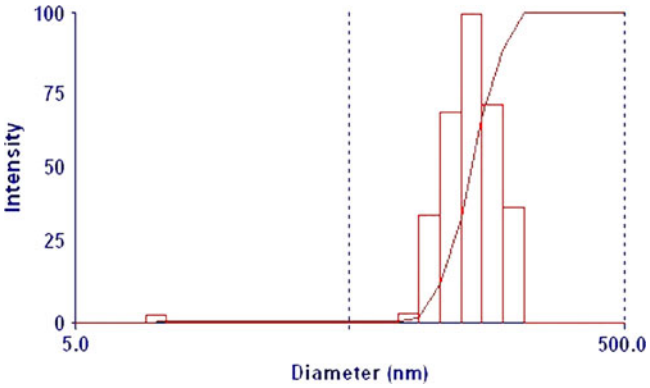

Fig. 1. Size distribution curve of sample No.5 (effective mean diameter 129.5 nm, PI=0.121)

the nozzle of a Buchi Mini Spray Dryer Model B290 (Buchi Laboratoriums-Technik AG, Flawil, Switzerland).The process parameters were set as shown in Table I. The solid NCs that had precipitated was accumulated into the bottom collector. The dried powder was weighed using Mettler Toledo XS 105 dual range balance (Mettler Toledo Inc., Columbus, USA) and stored in a sealed or capped glass container at room temperature.

Particle Size Determination

The particle size (Y_1, nm) and size distribution of IND loaded NCs was measured by dynamic light scattering (DLS, Brookhaven Instruments Corporation, Austin, TX, USA). DLS is a noninvasive, well-established technique for measuring the size of particles at nanometer scale. The spray-dried powder was redispersed in deionized water and sized at temperature of 25°C. The measurements were taken three times. The polydispersity index (PI) is given by the following equation:

$$\mathrm{PI} = \frac{K_2}{K_1^2} \tag{2}$$

Where K_1 is an effective mean diffusion coefficient while K_2 describes the relative width of the size distribution if normalized by K_1^2 (27).

According to National Institute Standard, a sample with a PI<0.5 was considered monodispersed (28).

Assessment of Process Yield

The process yield (Y_2, %) was calculated by the following equation:

$$\text{Yield}\ (\%) = \frac{W_r}{W_i} \times 100 \tag{3}$$

Where W_r was the weight of spray-dried powder collected in method section and W_i was the weight of total solids in the dispersion before spray drying.

Scanning Electron Microscopy

The scanning electron microscopy (SEM) technique was used to assess the morphology of NCs. Selected samples were analyzed by SEM for their surface morphology. The spray-dried samples were sonicated for 15 min to redisperse the particles in aqueous media. Samples were then pipetted onto a Nucleapore filter membrane and vacuum deposited. The membrane was mounted on a 1/2 in. SEM stubs with double-sticky carbon tape and secured with Ag paint around the perimeter of the membrane to the stub. The samples were sputter-coated (Emitech EMS575SX) with ~20 nm of Pt. The SEM picture was taken on a Hitachi S4700 Cold-cathode Field Emission Scanning Electron Microscope (Hitachi High-tech cooperation, Tokyo, Japan).

Transmission Electron Microscopy

The NCs were diluted in 2.5% uranyl acetate (UA), sonicated, and then 8 uL of the solution was put on a carbon coated grid, allowed to sit for 5 min. Excess solution was wicked off. Then 5% UA was put on the grid to increase the contrast. The grids were viewed under a JEOL JEM 1400 Transmission Electron Microscope (JEOL Inc., Peabody, USA), and photographed digitally on a Gatan axis-mount 2×2 k digital camera.

Statistical Analysis

The equations of the response values of size (Y_1) and yield (Y_2) were derived from the total result of the 11 runs in the four-factor two-level fractional factorial design. Analysis of variance (ANOVA) and lack-of-fit test were performed to ensure the model fit. Process parameters that had significant effects on the response were identified through Pareto chart. Irrelevant factors and interactions were deleted to obtain a

Table III. ANOVA Analysis for Both Responses

Response	Source	R^2	SS	DF	MS	*F* ratio	*P* value
Y_1 (Size)	Model		72,978.27	7	10,425.50	3.57	0.16
	Residual		8,747.67	3	2,919.90		
	Total	0.892	81,725.94	10			
Y_2 (Yield)	Model		288.80	7	41.26	28.88	0.0094
	Residual		4.28	3	1.43		
	Total	0.985	293.08	10			

SS sum of square, *DF* degree of freedom, *MS* mean sum of square, *F ratio* Lack-of-fit MS/Pure error MS, *P value* the area under *F* distribution curve to the right of tabulated critical *F* value

Table IV. Lack-of-Fit Analysis for Both Responses

Response	Source	SS	DF	MS	*F* ratio	*P* value
Y_1 (size)	Lack-of-fit	8,738.85	1	8,738.85	1,981.60	0.0005
	Pure error	8.82	2	4.41		
	Total	8,747.67	3			
Y_2 (yield)	Lack-of-fit	2.04	1	2.04	1.81	0.31
	Pure error	2.25	2	1.12		
	Total	4.29	3			

SS sum of square, *DF* degree of freedom, *MS* mean sum of square, *F ratio* Lack-of-fit MS/Pure error MS, *P value* the area under *F* distribution curve to the right of tabulated critical *F* value

reduced equation and used for optimization. After obtaining the optimized condition, a checkpoint analysis was performed to further confirm the model validation. The theoretical optimum condition for maximized process yield was given by the prediction model. This condition was validated in triplicates and checked for yield to ensure reproducibility.

Powder Flowability Analysis

The powder flowability was characterized via Carr's index and Hausner ratio through published method (29). Briefly, the bulk density was measured by placing approximately 1 g of powder under gravity into a calibrated measuring cylinder and record the volume occupied. The tapped density was further measured following established method by tapping the measuring cylinder on a wooden platform with an approximate amplitude of 20 mm until no further change in powder volume was observed (30,31). Carr's index and Hausner ratio were calculated through:

$$\text{Carr's Index}\ (\%) = \frac{(\text{Tapped Density} - \text{Bulk Density})}{\text{Tapped Density}} \times 100 \quad (4)$$

$$\text{Hausner ratio} = \frac{\text{Tapped Density}}{\text{Bulk Density}} \quad (5)$$

RESULTS AND DISCUSSION

Statistical Analysis and Optimization of Spray Drying Process

Table II described the responses obtained with the 2^{4-1} design for the particle size (Y_1), and the yield (Y_2), with additional information on PI. This data showed that NCs were indeed formed with the particle size ranging from 129.5 to 444.8 nm. Figure 1 showed a typical size distribution of the spray-dried NCs. The particle size ranging from 81.3 to 195.8 nm accounted for over 95% of the population. The size of the prepared NCs emulsion before spray drying varied from 149.6 to 439.2 nm. The particle size and size distribution are rarely the same as the original droplet. Higher available input energy levels may decrease the mean size of the droplet (32). Spray-dried NCs with similar size range were as reported in (18). The yield of NCs was from 14.1% to 31.1%. The PI of the sample ranged from 0.121 to 0.304. These 11 samples exhibited relatively large polydispersity, which may be due to aggregation of particles after preparation. Based on the analysis of the data, the equations for both response values were as follows:

$$Y_1 = 197.73 - 31.21X_1 + 22.61X_2 + 8.79X_3 - 27.79X_4 - 54.54X_1X_2 - 32.16X_1X_3 + 52.71X_1X_4 \quad (6)$$

$$Y_2 = 23.24 + 0.9X_1 - 0.15X_2 + 5.55X_3 + 0.9X_4 - 0.15X_1X_2 - 0.15X_1X_3 - 1.9X_1X_4 \quad (7)$$

Where the coded independent factors (X_i), which had the value of−1, 0, or +1 were: $X_1 = (X_{A1} - 145)/5$, $X_2 = (X_{A2} - 0.27)/0.09$, $X_3 = (X_{A3} - 525)/75$, and $X_4 = (X_{A4} - 90)/10$. The actual independent factors (X_{Ai}) were: X_{A1} for inlet temperature, X_{A2} for feed flow rate, X_{A3} for atomizing air flow, and X_{A4} for aspiration rate. The key measured response values were: Y_1 for particle size (nm) and Y_2 for yield (%).

The results from ANOVA and lack-of-fit analysis were given in Tables III and IV. For model validation, the *P* value obtained from ANOVA should be no more than 0.05, correlation coefficient (R^2) should be greater than 0.9, and the *P* value obtained from lack-of-fit should be no less than 0.05 (33). For Y_2, the *P* values in ANOVA analysis were less than 0.05, indicating the model adequately fit the data. The

Term	Estimate	Std Error	t Ratio	Prob>|t|
Atomizing air flow (L/h)(450,600)	5.55	0.422564	13.13	0.0010*
Inlet temperature (°C)*Aspiration rate (%)	-1.9	0.422564	-4.50	0.0205*
Inlet temperature (°C)(140,150)	0.9	0.422564	2.13	0.1230
Aspiration rate (%)(80,100)	0.9	0.422564	2.13	0.1230
Feed flow rate (L/h)(0.18,0.36)	-0.15	0.422564	-0.35	0.7461
Inlet temperature (°C)*Atomizing air flow (L/h)	-0.15	0.422564	-0.35	0.7461
Inlet temperature (°C)*Feed flow rate (L/h)	-0.15	0.422564	-0.35	0.7461

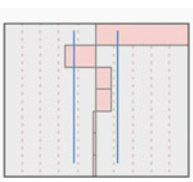

Fig. 2. Pareto chart showed the standardized effect of process parameters and their interaction on yield in Eq. 7. *X*-axis showed the *t* ratio of the variables. *Bars extending past the line* indicated values reaching statistical significance (α=0.05)

Table V. ANOVA and Lack-of-Fit Analysis for Eq. 9

Response	Source	R^2	SS	DF	MS	*F* ratio	*P* value
Y_2 (Yield)	Model		288.44	5	57.69	62.09	0.0002
	Residual		4.65	5	0.93		
	Total	0.984	293.09	10			
	Lack-of-fit		2.40	3	0.80	0.71	0.63
	Pure error		2.25	2	1.12		
	Total		4.65	5			

SS sum of square, *DF* degree of freedom, *MS* mean sum of square, *F ratio* Lack-of-fit MS/Pure error MS, *P value* the area under *F* distribution curve to the right of tabulated critical *F* value

correlation coefficient (R^2) was 0.985, indicating that the sum of square of the model accounted for over 90% of the total sum of square. The lack-of-fit test showed that the *P* value for Y_2 was >0.05, which indicated that at 95% confidence level, there was no lack of fit in the model. Therefore, we accept the model prediction for Y_2. On the other hand, since the *P* value of Y_1 in ANOVA was greater than 0.05, we rejected the model prediction for Y_1.

In both equations, the coefficient of the interaction terms (X_1X_2, X_1X_3, and X_1X_4) indicated how the response values changed when two variables simultaneously changed. The positive sign of the coefficient indicated a positive effect on size or yield while the negative signs showed a negative effect on those responses. In the study of Y_2, yield increased with X_1 and X_3 and X_4 settings, while the increase of X_2 had a negative effect on the NCs yield.

In order to visualize the significant variables in Eq. 7, a Pareto chart was constructed in Fig. 2, which indicates the main effect of the independent variables and interactions on Y_2. The values on the *x*-axis of the Pareto chart in Fig. 2 were the so-called standardized effects, which were in fact the *t* values. Those values were obtained based on the estimate of factor effect E_x, which was the coefficient in Eqs. 6, and 7. Then, *t* values were calculated based on the following equation:

$$t = \frac{|E_x|}{\mathrm{SE}_e} \tag{8}$$

Where $\mathrm{SE}_e$was the standard error of an effect (34). The obtained *t* values were compared to a tabulated critical *t* value (t_{critical}=3.18, as shown in the vertical line in Pareto chart). The critical *t* value was associated with the residual degree of freedom (residual *df* = number of runs − number of terms − 1)

Table VI. Results of ANOVA of Initial (Eq. 7) and Reduced (Eq. 9) Models for Y_2

ANOVA	*df*	SS	MS	*F* ratio
Regression				
Eq. 7	7	288.80	41.26	28.88
Eq. 9	5	288.44	57.68	62.09
Residuals				
Eq. 7	3	4.28 (C_1)	1.43 (D_1)	
Eq. 9	5	4.65 (C_2)	0.93	

$F_{\mathrm{cal}} = [(C_2 - C_1)/N_{\mathrm{TO}}]/D_1 = 0.13$, where N_{TO} was the number of terms omitted

and usually determined at significance level α=0.05. In Fig. 2, the absolute *t* values are represented by the length of the bar, and the critical *t* value is represented by the vertical line. Factors whose bar passes the vertical line (t_{critical} at P>0.05) had a significant impact on response values. From Fig. 2, it appears that among the four process parameters, only atomizing air flow had a significantly positive impact on the process yield. In order to further study the influence of process parameters on yield, statistically irrelevant interaction terms (X_1X_2, X_1X_3) were omitted from the initial model to generate a reduced model. The prediction equation of reduced model for Y_2 was:

$$Y_2 = 23.24 + 0.9X_1 - 0.15X_2 + 5.55X_3 + 0.9X_4 - 1.9X_1X_4 \tag{9}$$

The ANOVA and lack-of-fit analysis were shown in Table V. The R^2 value of the reduced model was 0.984. According to the same acceptability criteria, the results of R^2 value, ANOVA, and lack-of-fit indicated that omitting interaction terms did not impair the model validation. A comparison of initial and reduced models using ANOVA was shown in Table VI.

A Pareto chart of process parameters in reduced model is shown in Fig. 3 (t_{critical}=2.57, as shown in the vertical line). It is clear from Fig. 3 that increasing inlet temperature, aspiration rate, and atomizing air flow could significantly increase NC yield. These observations could be explained using the following basic operating principles of spray drying as described below.

The investigated inlet temperature (X_{A1}) ranged from 140°C to 150°C. Inlet temperature determined the temperature of the drying air at the contact of the feeding solution. The inlet temperature was measured before entry to the drying chamber, and it had influence on the amount of solvent that could be removed per unit time (13). Although the inlet temperature was close to the melting point of IND (158°C), it was reasonably speculated that the drug and/or oil component was not significantly degraded for the following reasons: (1) IND was shown to be relatively stable (with only 1.56% degradation) under high temperature and after melt-quench cooling process (35); (2) spray drying was a recognized method for the processing of heat-sensitive materials such as proteins and enzymes (8). This may be explained by the fact that the actual droplet temperature during the drying process was far lower than inlet temperature, and the exposure time was only 5–30 s (36). In this study, the outlet temperature during the spray drying of the NCs ranged from 48°C to 52°C. Moreover, it has been reported that usually the

Term	Estimate	Std Error	t Ratio	Prob>|t|
Atomizing air flow (L/h)(450,600)	5.55	0.340788	16.29	<.0001*
Inlet temperature (°C)*Aspiration rate (%)	-1.9	0.340788	-5.58	0.0026*
Inlet temperature (°C)(140,150)	0.9	0.340788	2.64	0.0459*
Aspiration rate (%)(80,100)	0.9	0.340788	2.64	0.0459*
Feed flow rate (L/h)(0.18,0.36)	-0.15	0.340788	-0.44	0.6782

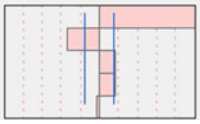

Fig. 3. Pareto chart showed the standardized effect of process parameters and their interaction on yield in Eq. 9. *X*-axis showed the *t* ratio of the variables. *Bars extending past the line* indicated values reaching statistical significance (α=0.05)

spray-dried particles reach a maximum temperature which is 15–20°C below the outlet temperature (8). It suggests that these substances were actually briefly exposed to an even lower temperature than the one observed experimentally. The overall thermal efficiency (η_{overall}) was defined as the fraction of total heat supplied to the dryer used in the evaporation process and can be approximately expressed as:

$$\eta_{\text{overall}} = \left(\frac{T_1 - T_2}{T_1 - T_0}\right) \times 100 \tag{10}$$

Where T_1 was inlet temperature, T_2 was outlet temperature, and T_0 was the atmospheric temperature (32). It showed an increase in thermal efficiency, which resulted from increasing the inlet temperature for fixed outlet and ambient temperature. Although the outlet temperature could not be predetermined theoretically, it was experimentally observed during the spraying process that it was stabilized between 48°C to 52°C. Overall, the inlet temperature had a positive effect on the process yield, because it raised the thermal efficiency leading to effective drying of the particles. Therefore, fewer particles were stuck to the drying chamber and cyclone and yield increased.

The feed flow rate (X_{A2}) was set from 0.18 to 0.36 L/h in this study. It was found in the preliminary study that higher feed rate (>0.36 L/h) would cause insufficient drying of the solvent leading to low yield. The phenomenon remains to be fully elucidated. However, according to Eq. 11, if increasing liquid feeding rate (V_{lf}) counteracts the effect of the atomizing air flow rate (V_{aa}), the decreasing air/fluid mass ratio ($n_{\text{a/f}}$) would result in insufficient drying. In this case, water may not be fully evaporated given the relative low outlet temperature and high water content in the nanosuspension. Although it was not found to be a significant factor in the range studied, the importance of controlling feed flow rate was elaborated through a previous study, as shown in the equation below in which ρ_{a} and ρ_{f} were the density of atomizing air and feed fluid intended to be atomized:

$$n_{\text{a/f}} = \frac{V_{\text{aa}} \times \rho_{\text{a}}}{V_{\text{lf}} \times \rho_{\text{f}}} \tag{11}$$

The coupling of the liquid feeding rate (V_{lf}) with the atomizing air flow rate (V_{aa}) and their influence on spray drying was defined by the air/fluid mass ratio ($n_{\text{a/f}}$) (37). The so-called air/fluid mass ratio represented the energy available for atomization, and decreasing $n_{\text{a/f}}$ would result in insufficient drying of particles (38). In this study, the difference between low and high settings of the feed flow rate appeared to have a statistically insignificant effect. Therefore, using the above Eq. 11, the energy available for atomization appeared here to be mainly dependent on atomizing air flow rate which positively impacted the process yield (Figs. 2 and 3). For example, indeed samples 5 and 11 (from Table II) did have relatively high yield (31.1% and 25.5%), but this fact might be mainly explained by the high value of V_{aa} (in Eq. 11) providing more effective drying energy. On the contrary, sample 10 with low V_{aa} value had a low yield of 14.1%.

The atomizing air flow (X_{A3}) in this study was set from 450 to 600 L/h. It referred to the gas flow in the nozzle. As shown in Eq. 11, this provided more energy available for atomization, causing the formation of a very large surface area owing to small droplet size that was exposed to the drying gas, which increased the drying efficiency (13). The droplet drying time τ_{d} could be described using the following Eqs. 12, and 13 (39):

$$\tau_{\text{d}} = \frac{d_0^2}{\kappa} \tag{12}$$

Where τ_{d} is the droplet drying time, d_0 is the initial diameter of the droplet, and κ is the evaporation rate:

$$\kappa = 8D_{\text{g}} \frac{\rho_{\text{g}}}{\rho_{\text{l}}} (Y_s(T_e) - Y_\infty) \tag{13}$$

Where D_{g} is the diffusion coefficient of the gas phase, ρ_{g} and ρ_{l} are density of the gas and liquid phases, respectively; Y_s and Y_∞ are the mass fraction of the solvent at droplet surface and in atmosphere, respectively; and T_e is the equilibrium temperature of the droplet.

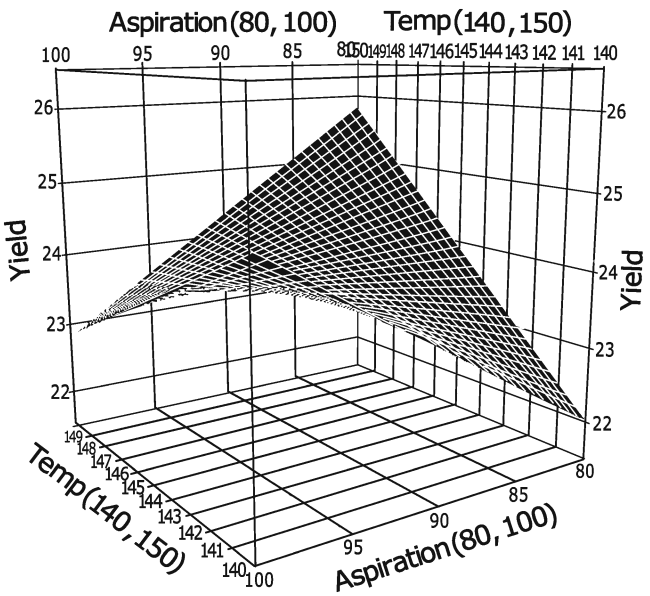

Fig. 4. The response surface plot showing effects of *inlet* temperature and aspiration air rate on the process yield

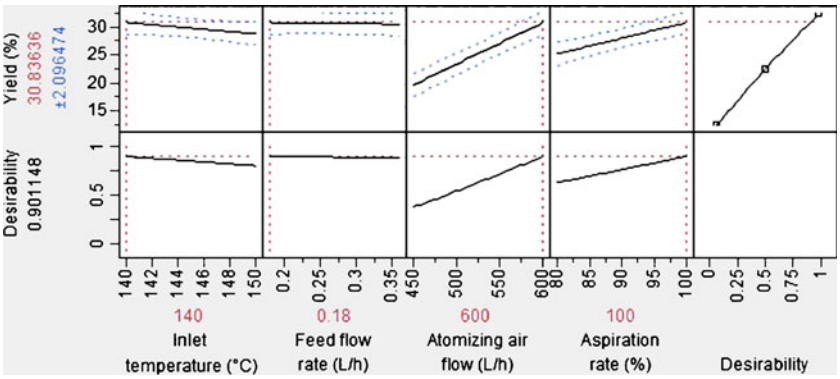

Fig. 5. Prediction and desirability plot showing the effect of process parameters on the yield

In a case where evaporation rate was fixed, higher atomizing air flow would help decrease initial diameter of the droplet and, therefore, significantly reduce drying time. Together with the effect of increasing air/fluid mass ratio as shown in Eq. 11, higher atomizing air flow rate would lead to effective drying of the particle and higher yield.

The aspiration air flow setting (X_{A4}) represented the drying gas flow rate in the spray dryer, which was the volume of drying air supplied per unit time. X_{A4} was set to 80% (low level) and 100% (high level) of the maximum drying air flow (35,000 L/h) of the Buchi B 290 spray dryer according to manufacturer specifications. The higher the aspiration setting, the shorter the particle transfer time (t_p) would be from the nozzle to the collector. When t_p was low, the interaction time between the particle and the drying gas would be relatively shorter. However, higher X_{A4} setting could increase the process yield by providing higher drying air velocity. Therefore, the increased centrifugal forces in the cyclone will increase cyclone efficiency (40) and X_{A4} had a positive effect as shown in Eq. 9.

The interaction between aspiration air flow and inlet temperature showed a significant negative effect on the process yield. As shown in Fig. 4, yield increases when inlet temperature and aspiration rate were increased. But after certain point, yield starts to decrease significantly, exhibiting an overall of negative interaction effect in Fig. 3. This could be explained by the antagonistic effect of both parameters. Increasing inlet temperature contributed to reducing droplet drying time τ_d, but increasing aspiration air flow rate could shorten t_p. If t_P was short enough to overwhelm the effect of faster dying (reduced τ_d), then the moisture content in the particle would be high enough which led to insufficient drying and forming sticky particles. These particles could be retained on the surface of drying chamber and decrease recovery of spray-dried NCs in the collector.

The relationship between the process parameters and the NCs yield was further investigated by constructing a prediction and desirability plot as shown in Fig. 5. The solid line indicates the prediction of process yield (%) as a function of the selected process parameters and the dotted lines around the solid lines indicates standard deviation. The concept of desirability function in optimization was described by Derringer and Suich (41) with desirability on the scale of 0 to 1, where 0 is not acceptable and 1 is the perfectly desirable response. Basically, the desirability was calculated as a function of the differences between fitted response value and the target value (42). Our goal was to maximize yield. The predicted yield was 30.8% with a desirability (d=0.90) which was close to the ideal value of 1. In Fig. 5, the predicted optimized condition can be translated as follows: inlet temperature 140°C, atomizing air low 600 L/h, feed flow rate 0.18 L/h, and aspiration air flow set at 100%.

Based on the reduced Eq. 9, a checkpoint analysis was performed to evaluate Y_2. The triplicate optimization points had an average yield of 32.5±2.4% (n=3), with a P value of 0.415 (α=0.05) compared to calculated value.

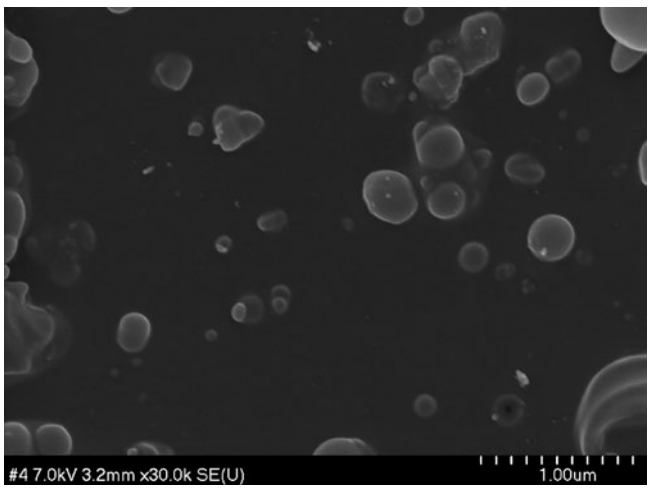

Fig. 6. Scanning electron microscopy image of IND-NC. *Scale bar* set at 500 nm

Physicochemical Characterization of the Oily Core Nanocapsules

The SEM image of spray-dried NCs is in Fig. 6. The particles exhibit a typical smooth spherical surface, and the size distribution is correlated well with the data measured by DLS. In transmission electron microscope (TEM) as in Fig. 7, areas of the specimen which block the beam cause fewer electrons to be transmitted to the camera, causing a dark field of view, which could be due to denser or thicker material, and lighter areas tend to be either less denser or thinner or both. Figure 7a, b shows the different internal structure of NCs and NP, exhibiting the electron density difference, which may be the result of the oily core nature of NCs. These data are consistent with our previous experiment for formulation variables optimization (43).

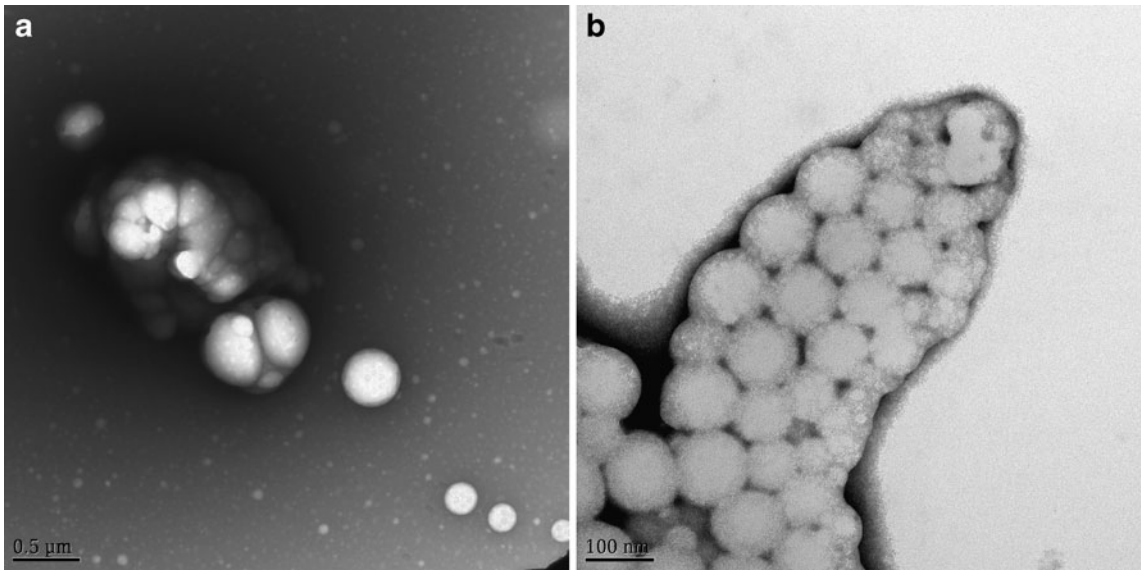

Fig. 7. Negative staining TEM image of IND-NC, scale bar set at 0.5 μm (**a**) and control NP, scale bar set at 100 nm (**b**)

Powder Flowability and Process Yield

The powder flowability of spray-dried NCs powder is summarized in Table VII. The bulk density and tapped density are measurements of the degree of packing or conversely the amount of space between the powder in the powder bed (29). A Hausner ratio value less than 1.20 is indicative of good flow, whereas a value greater than 1.5 indicates poor flow. The Carr's index value less than 25% indicates a fluid powder (good flow) whereas a value greater than 25% indicates a cohesive powder with poor flow (44). The results in Table VII exhibit poor powder flow, which might be due to insufficient drying related to the great amount of water added into the diffusion process. In spray-drying theory, increase in solid content of the feed solution (concentration of particles in the feeding solution) usually increases the bulk density of the powder and powder flow (32). The solid content in the feed solution tested in this study was relatively low (approximately 3.2% *w*/*w*), indicating a very high heat requirement for drying. Moreover, the powder flowability also improves with increasing particle size and greater particle sphericity (32), as the relatively small size of NCs could also contribute to poor powder flowability due to increased Van der Waals interaction. In practice, poor powder flowability was correlated with high moisture content in spray-dried powder shown in previous reports (45). With the relatively low solid content in feed solution used, there was high possibility that the moisture content was high in the spray-dried NCs thus suggesting a high chance of wet particle sticking to the drying chamber and the cyclone wall. This may explain the low yield in this process. Also, small particles such as those produced in this study might be much more easily carried out by Brownian motion in the drying gases, therefore bypassing the collector through the cyclone outlet and further explaining the low yield observed.

Table VII. Summary of Powder Flowability

Runs	Bulk density (g/ml)	Tapped density (g/ml)	Hausner ratio	Carr's index (%)
1	0.29	0.50	1.70	41.18
2	0.27	0.46	1.73	42.11
3	0.31	0.56	1.78	43.75
4	0.27	0.47	1.73	42.11
5	0.27	0.49	1.80	44.44
6	0.31	0.56	1.78	43.75
7	0.33	0.70	2.14	53.33
8	0.28	0.42	1.50	33.33
9	0.33	0.61	1.85	45.90
10	0.29	0.44	1.52	34.09
11	0.30	0.56	1.87	46.43

Influence of Process Parameters on Particle Size

Although the major use of FFED is in screening experiments, it was found in this study the FFED could not provide an adequate model to predict particle size. Since FFED neglects the polynomial effect of the individual factor and considers that two-factor interactions are confounded with each other (23), the inadequate fit of the model for particle size prediction might suggest the existence of a higher-order relationship in this case. It was found in the study, although the model did not fit the data well, smaller size could be obtained when the drying and atomization energy was high (high temperature, low feed rate, and high atomizing air flow according to Eq. 11), especially in the case of samples 5 and 9 with smallest size of 129 nm obtained with run 5 (Table II). It was well established in spray-drying technique that an increase in the energy available for atomization would reduce particle size (46). Experimental results from other investigators also confirmed this theory. For instance, Tajber *et al.* reported that the higher atomizing air flow was associated with smaller spray-dried microparticle (17), and this trend was also commonly observed (47,48). Mackaplow *et al.* studied the effect of disk speed on rotary spray congealing of microspheres. Disk rotation speed (similar to atomization air flow rate in spray drying) had the most significant effect on microsphere size, with higher speed yielding smaller congealed particles (14). Although feeding speed is high, particle size might be reduced due to higher centrifugal forces in spray congealing.

The impact of nozzle temperature was also studied in spray congealing process. Passerini *et al*. studied two different atomizing nozzles (wide pneumatic and air pressure type) in spray congealing process. Their data showed atomizing air pressure and nozzle temperature also had a positive effect on smaller particle size, which concur with spray-drying theory (15). Moreover, particle size usually increases as the feed concentration increases (8). The effect of temperature on the particle size is more material dependent (8). But these conclusions were not made based upon nanoparticles. Although FFED failed to provide an adequate model to predict the size, our objective was partially achieved, which was to produce spray-dried NCs under 220 nm suitable for sterile filtration, and i.v. injection. Alternative experimental design approaches such as Central Composite Design or Box–Behnken Design needs be studied to predict the effect of process parameters on size.

CONCLUSIONS

In this study, fractional factorial design enabled to investigate and optimize the yield of IND-loaded oily core NCs prepared by emulsion–diffusion technique and spray drying, which led to a yield of 30.8%. Statistical analysis proved the validity of the model and optimization process. Morphological analysis confirmed the existence of oily core structure. The powder flowability was low, which might be due to low feed solid concentration and small particle size. Spray-dried oily core NCs could serve as a template of novel nanocarrier for lipophilic drugs. The FFED shed light on future study of process optimization to predict NCs size in the field of nanoparticle manufacturing method using the emerging QbD concept.

ACKNOWLEDGMENTS

We are grateful to Dr. Elisabet Nalvarte (Division of Pharmacology, University of Missouri-Kansas City) for DLS experiments and the support of Louis Ross, Cheryl Jensen and Randy Tindall (Electron Microscopy Center, University of Missouri-Columbia) for the electron microscopy. We would also like to thank Dr. Marzelek (UMKC Division of Counseling and Education Psychology) for helpful discussion on statistical analysis and UMKC Writing Center for proof reading of this manuscript.

REFERENCES

1. Couvreur P, Tulkens P, Roland M, Trouet A, Speiser P. Nanocapsules: a new type of lysosomotropic carrier. FEBS Lett. 1977;84(2):323–6.
2. Lamprecht A, Ubrich N, Yamamoto H, Schafer U, Takeuchi H, Maincent P, *et al*. Biodegradable nanoparticles for targeted drug delivery in treatment of inflammatory bowel disease. J Pharmacol Exp Ther. 2001;299(2):775–81.
3. Rizkalla N, Range C, Lacasse FX, Hildgen P. Effect of various formulation parameters on the properties of polymeric nanoparticles prepared by multiple emulsion method. J Microencapsul. 2006;23(1):39–57.
4. Heurtault B, Saulnier P, Pech B, Proust JE, Benoit JP. A novel phase inversion-based process for the preparation of lipid nanocarriers. Pharm Res. 2002;19(6):875–80.
5. Limayem Blouza I, Charcosset C, Sfar S, Fessi H. Preparation and characterization of spironolactone-loaded nanocapsules for paediatric use. Int J Pharm. 2006;325(1–2):124–31.
6. Montasser I, Briancon S, Fessi H. The effect of monomers on the formulation of polymeric nanocapsules based on polyureas and polyamides. Int J Pharm. 2007;335(1–2):176–9.
7. Sollohub K, Cal K. Spray drying technique: II. Current applications in pharmaceutical technology. J Pharm Sci. 2010;99(2):587–97.
8. Broadhead J, Edmond Rouan SK, Rhodes CT. The spray drying of pharmaceuticals. Drug Dev Ind Pharm. 1992;18(11):1169–206.
9. Masters K. Spray drying-an introduction to principles, operational practice and applications. London: Leonard Hill; 1972.
10. Chan LW, Tan LH, Heng PW. Process analytical technology: application to particle sizing in spray drying. AAPS PharmSciTech. 2008;9(1):259–66.
11. Guterres SS, Weiss V, de Lucca Freitas L, Pohlmann AR. Influence of benzyl benzoate as oil core on the physicochemical properties of spray-dried powders from polymeric nanocapsules containing indomethacin. Drug Deliv. 2000;7(4):195–9.
12. Tewa-Tagne P, Briancon S, Fessi H. Preparation of redispersible dry nanocapsules by means of spray-drying: development and characterization. Eur J Pharm Sci. 2007;30(2):124–35.
13. Cal K, Sollohub K. Spray drying technique. I: hardware and process parameters. J Pharm Sci. 2009;99(2):575–86.
14. Mackaplow MB, Zarraga IE, Morris JF. Rotary spray congealing of a suspension: effect of disk speed and dispersed particle properties. J Microencapsul. 2006;23(7):793–809.
15. Passerini N, Qi S, Albertini B, Grassi M, Rodriguez L, Craig DQ. Solid lipid microparticles produced by spray congealing: influence of the atomizer on microparticle characteristics and mathematical modeling of the drug release. J Pharm Sci. 2010;99(2):916–31.
16. Naikwade SR, Bajaj AN, Gurav P, Gatne MM. Singh Soni P. Development of budesonide microparticles using spray-drying technology for pulmonary administration: design, characterization, *in vitro* evaluation, and *in vivo* efficacy study. AAPS PharmSciTech. 2009;10(3):993–1012.
17. Tajber L, Corrigan OI, Healy AM. Spray drying of budesonide, formoterol fumarate and their composites-II. Statistical factorial design and *in vitro* deposition properties. Int J Pharm. 2009;367(1–2):86–96.
18. Raffin Pohlmann A, Weiss V, Mertins O. Pesce da Silveira N, Staniscuaski Guterres S. Spray-dried indomethacin-loaded polyester nanocapsules and nanospheres: development, stability evaluation and nanostructure models. Eur J Pharm Sci. 2002;16(4–5):305–12.
19. Muller CR, Bassani VL, Pohlmann AR, Michalowski CB, Petrovick PR, Guterres SS. Preparation and characterization of spray-dried polymeric nanocapsules. Drug Dev Ind Pharm. 2000;26(3):343–7.
20. FDA. FDA guidance of industry: ICH Q8 Pharmaceutical development. Washington, DC: FDA; 2006.
21. Bei D, Marszalek J, Youan BB. Formulation of dacarbazine-loaded Cubosomes–part II: influence of process parameters. AAPS PharmSciTech. 2009;10(3):1040–7.
22. Bei D, Marszalek J, Youan BB. Formulation of dacarbazine-loaded cubosomes-part I: influence of formulation variables. AAPS PharmSciTech. 2009;10(3):1032–9.
23. Montgomery DC. Two-level fractional factorial designs. Design and analysis of experiments. 6th ed. Hoboken: Wiley; 2005.
24. Box GEP, Draper NR. Empirical model-building and response surface. New York: Wiley; 1987.
25. Showers MJ, Crosby EC. Somatic and visceral responses from the cingulate gyrus. Neurology. 1958;8(7):561–5.
26. Quintanar-Guerrero D, Allemann E, Doelker E, Fessi H. Preparation and characterization of nanocapsules from preformed polymers by a new process based on emulsification-diffusion technique. Pharm Res. 1998;15(7):1056–62.
27. Katzel U, Vorbau M, Stintz M, Gottschalk-Gaudig T, Barthel H. Dynamic Light Scattering for the Characterization of Polydisperse Fractal Systems: II Relation between Structure and DLS Results. Part Part Syst Charact. 2008;25:19–30.
28. Hackley V, Ferraris C. The use of nomenclature in dispersion science and technology, NIST Recommended Practice Guide: SP; 2001.
29. Nekkanti V, Muniyappan T, Karatgi P, Hari MS, Marella S, Pillai R. Spray-drying process optimization for manufacture of drug-cyclodextrin complex powder using design of experiments. Drug Dev Ind Pharm. 2009;35(10):1219–29.

30. Chevanan N, Womac AR, Bitra VS, Igathinathane C, Yang YT, Miu PI, *et al*. Bulk density and compaction behavior of knife mill chopped switchgrass, wheat straw, and corn stover. Bioresour Technol. 2010;101(1):207–14.
31. Ren Y, Yu C, Meng K, Tang X. Influence of formulation and preparation process on ambroxol hydrochloride dry powder inhalation characteristics and aerosolization properties. Drug Dev Ind Pharm. 2008;34(9):984–91.
32. Masters K. Spray drying in practice. Denmark: SprayDryConsult Intl. Aps; 2002.
33. Benita S, editor. Microencapsulation: methods and industrial applications. New York: Marcel Dekker; 1996.
34. Vander Heyden Y, Nijhuis A, Smeyers-Verbeke J, Vandeginste BG, Massart DL. Guidance for robustness/ruggedness tests in method validation. J Pharm Biomed Anal. 2001;24(5–6):723–53.
35. Patterson JE, James MB, Forster AH, Lancaster RW, Butler JM, Rades T. The influence of thermal and mechanical preparative techniques on the amorphous state of four poorly soluble compounds. J Pharm Sci. 2005;94(9):1998–2012.
36. Deasy PB. Microencapsulation and related drug processes. New York: Dekker; 1984.
37. Li Z, Li Q, Simon S, Guven N, Borges K, Youan BB. Formulation of spray-dried phenytoin loaded poly(epsilon-caprolactone) microcarrier intended for brain delivery to treat epilepsy. J Pharm Sci. 2007;96(5):1018–30.
38. Lee G. Spray-drying of proteins. Pharm Biotechnol. 2002;13:135–58.
39. Vehring R. Pharmaceutical particle engineering via spray drying. Pharm Res. 2008;25(5):999–1022.
40. Maury M, Murphy K, Kumar S, Shi L, Lee G. Effects of process variables on the powder yield of spray-dried trehalose on a laboratory spray-dryer. Eur J Pharm Biopharm. 2005;59(3):565–73.
41. Derringer G, Suich R. Simutaneous optimization of several response variables. J Qual Technol. 1980;12:214.
42. NIST/SEMATECH. e-Handbook of Statistical Methods [cited 2010 Apr.08]. Available from: http://www.itl.nist.gov/div898/handbook/.
43. Zhang T, Youan B.B.C. Optimization of formulation variables affecting spray dried oily core nanocapsules by response surface methodology. J Pharm Sci. 2010 (in press).
44. Gonnissen Y, Remon JP, Vervaet C. Effect of maltodextrin and superdisintegrant in directly compressible powder mixtures prepared via co-spray drying. Eur J Pharm Biopharm. 2008;68 (2):277–82.
45. Dawoodbhai S, Rhodes CT. The effect of moisture on powder flow and on compaction and physical stability of tablets. Drug Dev Ind Pharm. 1989;15(10):1577–600.
46. Masters K. Spray drying handbook. 4th ed. Chichester: Wiley; 1985.
47. Chawla A, Taylor KMG, Newton JM, Johnson MCR. Production of spray dried salbutamol sulfate for use in dry powder aerosol formulations. Int J Pharm. 1994;108:233–40.
48. Stahl K, Claesson M, Lilliehorn P, Linden H, Backstrom K. The effect of process variables on the degradation and physical properties of spray dried insulin intended for inhalation. Int J Pharm. 2002;233(1–2):227–37.